Dynamical Models for the Ion Channel Switch (ICS) Biosensor

by

Sahar Moradi Monfared

B. A. Sc., The University of British Columbia, 2007

A THESIS SUBMITTED IN PARTIAL FULFILLMENT OF
THE REQUIREMENTS FOR THE DEGREE OF

MASTER OF APPLIED SCIENCE

in

The Faculty of Graduate Studies

(Electrical and Computer Engineering)

THE UNIVERSITY OF BRITISH COLUMBIA

(Vancouver)

August, 2010

Abstract

This thesis derives dynamical models that explain the operation of a solid phase immunoassay biosensor, the Ion Channel Switch (ICS) biosensor. The ICS biosensor unlike similar biosensors admits multiple surface chemical reactions which make the mathematical models significantly more complex than models used to describe alike biosensors. A two dimensional partial differential equation describes the distribution of the analyte through out the flow chamber. The interaction of analyte and the immobilized species at the biosensor electrode is modelled through the boundary condition at the bottom of the flow chamber. This boundary condition couples the partial differential equation to a set of nonlinear ordinary differential equations which are used to describe the surface chemical reactions. This model produces accurate results particularly when the rate of transport of analyte to the biosensor surface is comparable to the rate of reactions occurring at the biosensor surface. However, when the rate of mass transport is much faster than the reaction rates, the dynamics of the ICS biosensor can be accurately described by a system of nonlinear ordinary differential equations in which analyte concentration is assumed constant. Accuracy of the derived mathematical models are verified by comparing the simulated biosensor response to that obtained from an experimental run of the ICS biosensor.

Preface

The operation of the ICS biosensor as well as the mathematical modelling described in Chapter 3 were published in the IEEE Transactions on Nanotechnology (2010, 9(3): $313-321$), entitled *"Ion-Channel Biosensors Part II: Dynamic Modeling, Analysis and Statistical Signal Processing"* as well as in the Proc. of 7th IEEE International Workshop on Genomic Signal Processing and Statistics (Minnesota, May 2009), entitled *"Stochastic Modeling and Signal Processing of Nano-Scale Protein-Based Biosensors"*. S.M. Monfared, the thesis author, was one of the principle authors who performed most of the research, analyzed data and prepared the manuscript. Dr. Vikram Krishnamurthy, S.M. Monfared's supervisor, was the other co-author and provided close guidance on performing the above research. Dr. Bruce Cornell, the co-author of this study provided experimental data used to perform model evaluation in Chapter 4.

The electrical modelling of the ICS biosensor in Chapter 3 appears in the Proc. of of 48th IEEE Conference on Decision and Control (Shanghai, December 2009), entitled *"Reconfigurable Ion- Channel based Biosensor: Input Excitation Design and Analyte Classification"*. S.M. Monfared was the principle author and Dr. V. Krishnamurthy, and Dr. B. Cornell were the co-authors.

Table of Contents

List of Tables

List of Figures

List of Abbreviations

ICS	Ion channel switch biosensor
BLM	Bilayer lipid membrane
gA	gramicidin A
hCG	human chorionic gonadotropin
IgG	Immunoglobin G
ELISA	Enzyme Linked Immunosorbent Assay
Fab	Fragment antigen binding portion of antibody

Acknowledgements

I would like to thank my supervisor, Dr. Vikram Krishnamurthy, for his constant support and guidance. I would also like to thank my collaborator, Dr. Bruce Cornell, for his advice and assistance and for providing the experimental data in this thesis. Thanks to my sister Nasim for her patience in explaining to me the unfamiliar biological concepts and for her constant encouragement. Thanks to my family for their unconditional support and love. Finally thanks to my friends and colleagues.

Dedication

To Nasim, Saman, Leyli, Mojan and Nader

Chapter 1

Introduction

1.1 Dynamic Models for Biosensors

A biosensor converts a biological binding event to a measurable signal. It comprises a biorecognition molecule integrated with a signal transducer. To achieve selectivity towards target/analyte molecules it borrows from nature the recognition properties of molecules such as enzymes, antibodies, peptides or DNA [3], [4], [5]. The biorecognition/receptor molecules bind to the target/analyte molecules which cause a physio-chemical change in the biorecognition unit. The transducer then converts the physio-chemical change into a concentration dependent signal which is picked up by the measurement device. A good review of various transducers in biosensor technology is provided in [6].

In recent years there has been significant growth in the area of research and development of new and improved biosensors. Biosensors find applications in areas such as biotechnology, chemistry, physics, medicine and food industry. For example biosensors have long been utilized to sense glucose levels in both medical and industrial applications [7]. Another important medical application is urea biosensors which are essential in portable hemodialysis systems for treating patients with renal disorder [8].

Biosensors, such as BIACORE, also provide a popular method for the analysis of reaction rate constants in biomolecular interactions. These types of biosensors utilize a flow chamber, with the bio-recognition molecules immobilized on the sensor surface and the sample containing analyte/target molecules flowing through the chamber [9], [10]. By studying the time course of binding of the reactants and assuming an underlying mathematical model that describes the dynamics of association and dissociation of the analyte and the receptor molecules, the intrinsic reaction rate constants can be estimated [10], [11].

The analytic signal produced by the transducer of such biosensors is the result of the interplay of many complex phenomena including the chemical kinetics as well as the mass transport effects. Therefore, an important step in the design and implementation of solid phase immunoassay biosensors is understanding the dynamics of association and dissociation of analyte molecules with the immobilized species on the biosensor surface . Also since biosensors in most chemical and immunodiagnostic applications incorporate a flow chamber, transport effects such as advection and diffusion of analyte to the biosensor surface play important roles in the analysis and design of such assays. These effects need to be incorporated in the mathematical models that reflect the chemical dynamics of the biosensor. If we can relate the events occuring in a biosensor to equations that describe them, it would be possible to design new systems without extensive experimentation.

1.2 Contributions and Results

In this dissertation, dynamical models that describe the operation of a fluidic-based solid phase immunoassay biosensor, called the Ion Channel Switch (ICS) biosensor, are derived. The Ion Channel Switch (ICS) biosensor exploits the molecular switching mechanism of ion channels to detect target molecular species of interest across a wide range of applications with concentrations as low as 10fM [12]. It is composed of gramicidin A (gA) ion channels embedded in a lipid bilayer, which is tethered to a gold electrode as shown in Fig. 1.1. Gramicidin A ion channels are produced by the soil bacterium Bacillus brevis and consist of two halves or monomers. When the two monomers align they form a longer conducting pipe known as a dimer which allows ions to pass through. Tethered to the gold electrode as well as attached to the free moving gA monomers in the top layer of the lipid bilayer are binding sites or receptor molecules. If the sample solution contains target analyte molecules, they are carried to the biosensor surface by advection and diffusion. The arrival of analyte molecules at the biosensor surface, cross-links antibodies attached to the mobile outer layer channels, to those attached to membrane spanning lipid tethers, Fig. 1.1 (c). This disrupts the ability of gA monomers to align and form conducting dimers. Therefore conductance of the membrane decreases. The resulting decrease in current signals the presence of analyte. Therefore channel conductance, G, is directly proportional to the concentration of the dimers present in the biosensor D. The evolution of the dimer concentration in the biosensor is a function of analyte concentration present in the sample solution. As a result

the decay in biosensor conductance is a function of analyte concentration.

In this dissertation the qualitative description provided above is translated to mathematical models that can be used to simulate the biosensor response. We use a two dimensional advection diffusion partial differential equation (PDE) subject to a mixture of Neumann and Dirichlet boundary conditions to describe the distribution of analyte concentration through out the flow chamber. The interaction of analyte molecules with the immobilized species on the biosensor surface is modelled through the boundary condition posed at the bottom of the flow chamber. This boundary condition couples the advection diffusion PDE to a set of nonlinear ordinary differential equations (ODE) that model the evolution of the concentration of the immobilized species on the biosensor surface.

The PDE model describes the operation of the biosensor under all operating conditions. The operating condition of the ICS biosensor is defined by the concentration of analyte present in the sample solution, the binding site density at the biosensor surface, and the flow rate of the sample solution through the flow chamber. Depending on the values of these variables, the biosensor operates in one of two regimes; reaction-rate-limited or mass-transport influenced regimes. Reaction-rate-limited region of operation is entered when high analyte concentration, high flow rate and relatively low binding site density is used. Mass-transport influenced region is entered when low analyte concentration, high binding site density and low flow rates define the operating condition of the biosensor. In the mass-transport influenced region the rate of transport of analyte molecules to the biosensor surface is comparable to the surface reaction rates. In this region, in order to

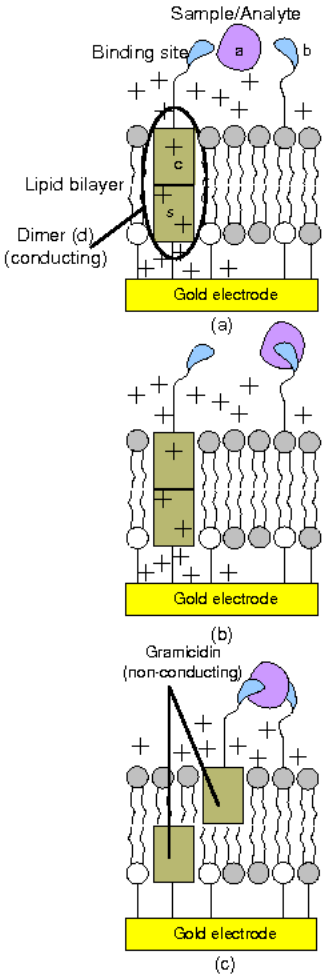

Figure 1.1: Large analyte transduction mechanism. Analyte (purple) is denoted by a, binding site (blue) is denoted by b, free moving gA monomers are denoted by s and c. The binding of analyte to the binding site causes the conformation of gramicidin A to shift from conductive dimers (a) to non-conductive monomers (c). This causes a loss of conduction of ions across the membrane. The scale can be visualized by the fact that the tethered lipid bilayer is 4nm thick. (a) gA in dimer form before the binding of analyte to the binding site. (b) Analyte molecules binding to binding site consisting. (c) gA monomer in the top leaflet of the lipid bilayer binding to the analyte-binding site complex, thus disrupting the dimer formation.

accurately simulate the biosensor response, the two dimensional PDE needs to be solved numerically. Under reaction-rate-limited operating conditions the rate of transport of analyte molecules to the biosensor surface is much faster than the surface chemical reactions. Therefore, it is reasonable to assume constant analyte concentration through out the flow chamber. The assumption of constant analyte concentratoin in this region, decouples the PDE from the system of ODEs. Therefore the biosensor dynamics are described by a system of nonlinear ODEs in the reaction-rate-limited region of operation.

1.2.1 Main Contributions

The main contributions of this dissertation can be summarized as below:

- *Modelling of Biosensor Electrical Response :* In Section 3.1 we give a complete model description of the electrical response of the biosensor. The electrical dynamics of the ICS biosensor are described by an equivalent second order linear system. In the equivalent electrical model, a capacitor in parallel with a resistor account for the electrical properties of the lipid bilayer with embedded gA ion channels. The helmholtz and diffuse layer capacitances are accounted for by a single capacitor and the electrolyte resistance is also considered.

- *Chemical Reaction Network of the ICS Biosensor :* The chemical kinetics detail how the biosensor responds to analyte molecules – from analyte molecules binding to the receptors to the eventual disruption of the ability of gramicidin molecules to form dimers. There are four pri-

mary chemical species in the ICS biosensor, analyte, binding site, free moving gA monomers and tethered gA monomers. The four primary species combine according to a set of reversible chemical reactions to form four complexes or products. Therefore, we use a total of seven reversible reactions to describe the chemical reaction network of the ICS biosensor. From the chemical reaction network and the law of mass action we can derive a system of nonlinear ODEs to describe the evolution of the concentration of the chemical species in the ICS biosensor.

- *Analyte Flow and Analysis of Biosensor Dynamics :* The distribution of analyte concentration through out the flow chamber depends on the bulk analyte concentration, the binding site density and the flow rate of the sample solution. These parameter values define the operating condition of the ICS biosensor. These operating conditions in turn distinguish two regions of operation for the biosensor; the reaction-rate-limited and the mass-transport influenced regions. High bulk analyte concentration, relatively low binding site density and high flow rate, push the operation of the ICS biosensor into the reaction-rate-limited region, where analyte concentration can be assumed constant. In this region the chemical kinetics are modelled by the system of nonlinear ODEs. The ODE model is derived from the chemical reaction network of the biosensor with analyte concentration taken to be constant and equal to the bulk analyte concentration. On the other hand, low analyte concentration, high binding site density and low flow rate,

push the biosensor operation into the mass-transport influenced region, where the distribution of analyte concentration in the flow chamber is given by a two dimensional advection diffusion PDE subject to complex boundary conditions. In particular the boundary condition at the biosensor surface reflects the interaction of analyte molecules with the immobilized species. This boundary condition models the rate by which analyte molecules are grabbed by the immobilized species. This rate is a function of the concentration of all surface chemical species. Thus a full description of the dynamics of the biosensor in this region is obtained by numerically solving the system of nonlinear ODEs coupled with the 2-D advection diffusion PDE. Comparison of the simulated biosensor response from the two models under appropriate operating conditions to experimental data obtained from the ICS biosensor verifies the accuracy of the mathematical models, as shown in Chapter 4.

1.2.2 Limitations

In this dissertation we have used concepts from physics and chemistry to construct a "white-box" model for the chemical kinetics of the ICS biosensor. Although we have studied the operation and construction of the ICS biosensor in order to arrive at dynamical models, we have not been involved in the implementation of the biosensor. Nor have we been involved in running experiments on the biosensor. In fact all the experimental data used to verify the accuracy of the derived models in Chapter 4 is provided by SDX research which is the company currently producing the ICS biosensor.

Our main focus thus far has been to derive models that could simulate the biosensor response accurately. We have only analyzed the proposed dynamical models by comparing the experimental response of the ICS bisoensor to the simulated response from each model. However, we have not performed error analysis. There is room for model optimization through minimizing the error between the experimental and simulated responses.

1.2.3 Related Publications

1. V. Krishnamurthy, **S. M.Monfared** and B. Cornell, *Ion-Channel Biosensors Part II: Dynamic Modeling, Analysis and Statistical Signal Processing*, in IEEE Transactions on Nanotechnology, Volume 9, Issue 3, pp. $313 - 321$, 2010.

2. **S. M.Monfared**, V. Krishnamurthy and B. Cornell, *Reconfigurable Ion- Channel based Biosensor: Input Excitation Design and Analyte Classification*, in Proc. of of 48th IEEE Conference on Decision and Control (CDC), Shanghai, China, December 2009.

3. **S. M.Monfared**, V. Krishnamurthy and B. Cornell, *Stochastic Modeling and Signal Processing of Nano-Scale Protein-Based Biosensors*, in Proc. of 7th IEEE International Workshop on Genomic Signal Processing and Statistics (GENSIPS), Minnesota, USA, May 2009.

1.3 Background and Related Work

The literature on biosensors is vast. Neher provides an interesting overview of the interface between ion channels and microelectronics [13]. Several companies/research groups have developed biosensors based on synthetic lipid monolayers and bilayers. For example OhmX Corporation is currently developing a reagentless biosensor system using self assembled monolayers tethered to a gold surface for the electronic detection of biomarkers in clinical samples [14]. Stochastic signal analysis has been employed by Bayley's group at Oxford and has made substantial contributions in advancement of ion channel biosensors [15], [16]. The detection of single gramicidin channel currents in a tethered membrane is described in [14]. Here we focus on the ICS biosensor currently being developed by Surgical Diagnostics Pty Ltd as an important example of an ion channel based biosensor. Below we provide a review of related work in biosensors involving ion channels and tethered lipid membranes.

The first attempt at developing a practical membrane-based biosensor device was reported in [17]. The poor stability of the receptor-membrane complex limited the range of applications of the device. One of the first examples of a functionally active biomimetic surface was reported in [18], in which an active cytochrome C was incorporated into a tethered membrane.

The stabilization of the *bilayer lipid membrane* (BLM) has been a central theme in the development of ion channel biosensors [19]. Many strategies have been developed. The primary focus has been on physisorbing or chemically attaching a layer of hydrocarbon to a silicon [20], hydrogel [21],

polymer [22] or metal surface [23]. Subsequently a second layer of mobile lipids is fused onto the tethered monolayer to form a tethered bilayer lipid membrane. Earlier works on BLM stabilization is reviewed in [24] and [25]. In [26] peptide nanotubes have been fabricated within a supported self assembled monolayer. The ICS biosensor employs an alkane disulphide bond to stabilize the bilayer lipid membrane at the electrode surface.

A key requirement of an ion channel biosensor is to engineer a switching mechanism that modulates the flow of ions when an analyte is detected [27]. Mechanisms range from anti-channel antibodies that disrupt ion transport [28], to molecular plugs that block the channel entrance [29]. Ompf porin channels from E coli, were incorporated into a tethered BLM and their conduction modulated using the channel blocker colicin [30]. All mechanisms proposed so far have had a very limited range of application and require re-engineering for each new analyte. The ICS, whilst using ion channel transduction provides a mechanism that may be adapted to many different classes of target molecules.

The objective of this thesis is to provide mathematical models that allow one to predict kinetic and electrical characteristics of the ICS biosensor under various operating conditions. Such models provide insight into the operation of the device as well as allowing one to optimize the operation of the device.

The equivalent electrical model we introduce in Section 3.1 for the lipid membrane, interfacial capacitance and electrolyte resistance is similar to that used in electro-physiological models of cell membranes [31]. The conceptual idea behind electro-physiological models originates from the work of Cole, who pioneered the notion that cell membranes could be likened to

an electronic circuit [32]. The chemical kinetics in Section 3.2.1 result in a system of nonlinear ordinary differential equations. The book [33] is an excellent example of such chemical kinetics and binding.

The mass-transport dynamics (partial differential equation) coupled with the chemical kinetics of Section 3.2.1 result in an advection diffusion partial differential equation with Neumann and Dirchlet boundary conditions [9, 34, 35]. Similar formulations for binding and dissociation between a soluble analyte and an immobilized ligand are studied in [36]. In [9, 11], mass-transport dynamics are formulated for a two compartment model where analyte molecules move between the two compartments. Goldstein et al. discuss the accuracy and theoretical basis of different models for mass-transport effects in the binding of analytes in [35]. Similar models have been adopted in [37] where mathematical models describing the dynamics of a lateral flow reactor which consists of a flat, porous membrane to which ligands are immobilized are derived. Similarly in [38] analytical solutions of the differential equation which governs the fluid flow in the flow channel of an electrochemical detector are found. The model utilized to explain the dynamics of the flow is simplified by neglecting longitudinal diffusion and analytical solutions are only possible under steady state assumptions. Also in [39] and [40] a set of partial and ordinary differential equations coupled through the boundary conditions are used to study the transport and kinetic processes affecting the operation of the biosensor BIACORE.

1.4 Thesis Organization

In Chapter 2 a brief introduction to the ICS biosensor technology is provided. Section 2.1 presents a terse description of the structure and operation of gramicidin A ion channels. In Sections 2.2 and 2.3 the construction and operation of the ICS biosensor are explained. In Chapter 3, mathematical models describing electrical as well as chemical dynamics of the biosensor under various operating conditions are derived. In Section 3.1, the electrical dynamics of the ICS biosensor are described by an equivalent electrical circuit. In Section 3.2.1 the chemical reaction network of the ICS biosensor is modelled by a system of nonlinear ordinary differential equations. In Section 3.2.2 experimental response of the biosensor to different analyte concentrations are presented. In Section 3.3 two regions of operation are distinguished for the ICS biosensor; the reaction-rate-limited and the mass-transport influenced regions. In Section 3.3.1 the operation of the ICS biosensor in the reaction-rate-limited region is described and a motivating example is presented. In Section 3.3.2, the partial differential equation describing the dynamics of the ICS biosensor under all operating conditions especially the mass-transport influenced region is derived. In Chapter 4 the accuracy of the derived mathematical models are verified by comparing the simulated data to the experimentally obtained data from the ICS biosensor. Finally Chapter 5 summarizes the project findings, provides concluding remarks as well as briefly describes the possible future work in this project.

Chapter 2

Ion Channel Switch (ICS) Biosensor

In biological sensing systems a receptor protein is typically coupled to a switchable ion channel embedded in a lipid bilayer surrounding the cell. The biological sensing system detects the presence of target molecules by monitoring the electrical changes of the cell membrane. These electrical changes result when target molecules bind to the receptor molecules thus changing the conductivity of the embedded ion channels [41]. One binding event typically triggers the passage of $10^7 - 10^8$ ions, leading to a significant and measurable change in the conductivity of the membrane.

Certain advantages of biological sensing systems such as large amplification that results from a single binding event as well as the simplicity and robustness of this type of detection make this approach particularly interesting in the development of biosensors. However, to make the biosensor as generic as possible it must be able to detect a wide range of molecules. Therefore unlike biological sensing systems in nature, where both the receptor molecule and the ion channel are included in the same assembly, in anlaytical biosensors the ion channels and the receptor molecules must be

seperate units [42]. Therefore it makes sense to use a simple ion channel whose switching mechanism is independent of the type of analyte and make the biosensor sensitive to a particular analyte molecule by using appropriate receptors. An example of such ion channels is the gramicidin A ion channel, which is used in the developement of the ICS biosensor. In the following sections brief introductions to gramicidin A ion channels as well as the operation and construction of the ICS biosensor are provided.

2.1 Gramicidin A Ion Channels

Biological ion channels are water-filled sub-nano-sized pores formed by protein molecules in the membranes of all living cells [31, 43]. Ion channels play a crucial role in living organisms by selectively regulating the flow of ions into and out of a cell thereby controlling the cell's electrical and biochemical activities.

Gramicidins are a family of ion channels produced by the soil bacterium Bacillus brevis, and consist of alternating L- and D-amino acids [44]. Because they are small, readily available and easily modified chemically , gramicidin is often used as a model pore to study ionic channels. It comprises of two gramicidin peptides or monomers. When the two peptides are linked head to head by hydrogen bonds they form a conducting pore known as a dimer [44]. The dimer has a pore diameter of 4$\mathring{A}$ and a length of about 25$\mathring{A}$. Gramicidin ions are selective to monovalent cation and have conductance of about 10^7 ions per second.

2.2 Construction

The low molecular weight bacterial ion channel gramicidin has been used, (see [12], [45], see also [1] for a review), as the basis of a biosensor platform with a range of applications for the detection of low molecular weight drugs, large proteins and micro-organisms [46], [47] . The ICS biosensor employs a lipid bilayer tethered via hydrophilic spacers to a gold surface.

The membrane stability is primarily enhanced by tethering the inner membrane leaflet to the gold surface. However additional stability is achieved by substituting a major fraction of the tethered lipids with archaebacterial lipids. These are lipids modeled on constituents found in bacteria capable of surviving extremes of temperature and hostile chemical environments. Characteristics of these lipids are that the hydrocarbon chains span the entire membrane and that all ester linkages are replaced with ethers [48], [49]. Bilayer Lipid Membrane (BLM) films have previously been formed from archaebacterial lipids and resulted in membranes that are stable to temperatures in excess of 90°C [50]. A stable membrane incorporating ion channels can be self-assembled on a clean, smooth gold surface using a combination of sulphur-gold chemistry and physisorption [51]. Most studies of the ICS biosensor have used antibody Fab fragments as the receptor; however, the approach has also been demonstrated to operate using oligonucleotide probes, heavy metal chelates and cell surface receptors.

The construction of the ion channel biosensor developed by [12] involves sophisticated concepts in biochemistry. However, for our purposes its structure can be simply described as follows. First an artificial tethered lipid

monolayer is constructed containing tethered gramicidin channels. Then a second outer mobile monolayer comprising of lipids and gramicidin channels is introduced. These components self-assemble in water to form a lipid bilayer that mimics a cell membrane. The gramicidin channels act as sub-nano-sized pipes that move randomly along the outer monolayer of the bilayer. The channels in the inner layer are tethered and hence cannot move. As the mobile gramicidin channels in the outer layer diffuse, occasionally a channel in the outer layer will align exactly with a channel at the inner level of the membrane, thereby forming a single longer pipe known as a dimer. When a dimer forms, ions travel along it, thereby resulting in a small current. At any given time instant, several such pairs of pipes can align (forming dimer) or dis-associate (breaking dimers), since the outer layer diffuses randomly. Therefore the current recorded at the output of the biosensor is a random process. In the construction of the biosensor, specific antibodies (binding sites/receptor molecules) that recognize specific analyte molecules are attached to the mobile outer layer channels as well as to the gold electrode, see Fig. 2.1.

2.3 Operation

In the same manner that an ELISA sandwich assay may be developed based on a complementary antibody pair, the ICS biosensor may be adapted to the detection of any antigenic target for which a suitable antibody pair is available. For example in order to detect the pregnancy hormone (human chorionic gonadotropin (hCG)), the antibody Immunoglobin G (IgG) can

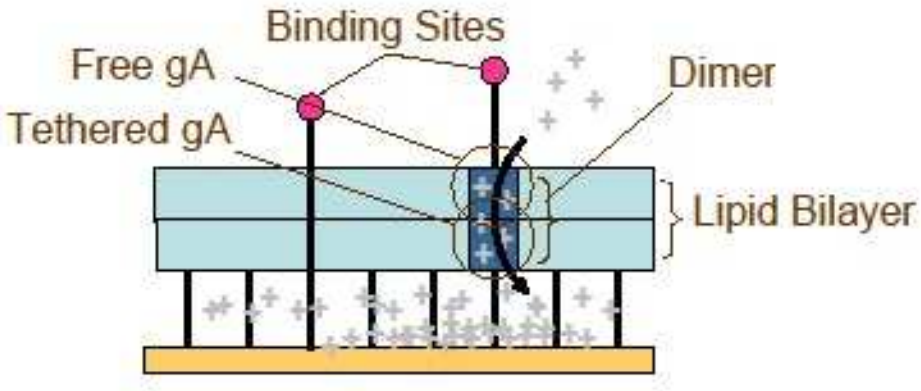

Figure 2.1: ICS biosensor structure, including the lipid bilayer tethered to the gold electrode and the binding sites tethered to the free moving gA monomers as well as to the gold electrode.

be used as the receptor molecules of the biosensor. The bacterial ion channel gramicidin A is assembled into a tethered lipid membrane and coupled to an antibody, targeting a compound of diagnostic interest. Solution that may or may not contain the analyte is introduced. If no analyte molecules are present, the biosensor operates as outlined in Section 2.2. On the other hand, if the solution contains the target analyte, then the arrival of analyte cross-links antibodies attached to the mobile outer layer channels, to those attached to membrane spanning lipid tethers, Fig. 1.1. This disrupts the ability of gA monomers to align and form conducting dimers. Therefore conductance of the membrane decreases. The resulting decrease in current signals the presence of analyte. Therefore channel conductance, G, is directly proportional to the concentration of the dimers present in the biosensor, D. The evolution of the concentration of the dimers in the biosensor is a function of the concentration of the analyte present in the sample solu-

tion. As a result the decay in biosensor conductance is a function of analyte concentration.

Applying a small alternating potential between the gold and the reference electrode in the test solution generates a charge at the gold surface which causes electrons to flow in an external circuit. Therefore the output current of the ICS biosensor can be measured.

Chapter 3

Modeling the Dynamics of the ICS Biosensor

3.1 Electrical Dynamics of the Biosensor

The ICS biosensor can be viewed as a biological transistor. Fig.3.1(a) illustrates the equivalent circuit of the biosensor before and after the detection of analyte. Fig.3.1(b) details the components of the equivalent circuit. The resistor $1/G$ models the *biosensor resistance* and increases with the presence of analyte. C_1 denotes the capacitance of the membrane while C_2 denotes the interfacial capacitance of the gold substrate [52]. R_2 denotes the resistance of the electrolyte and its value varies depending on the type of electrolyte and the dimensions of the return path in the bathing solution. In a flow chamber, the dimensions of the return path can be sufficiently small so that R_2 becomes significant.

The values of C_1, C_2, R_1 and R_2 are functions of electrode area. Electrodes in the 2009 generation ICS biosensors have an area of 0.03cm^2. Therefore typical values for the equivalent electrical circuit components are listed in Table 3.1.

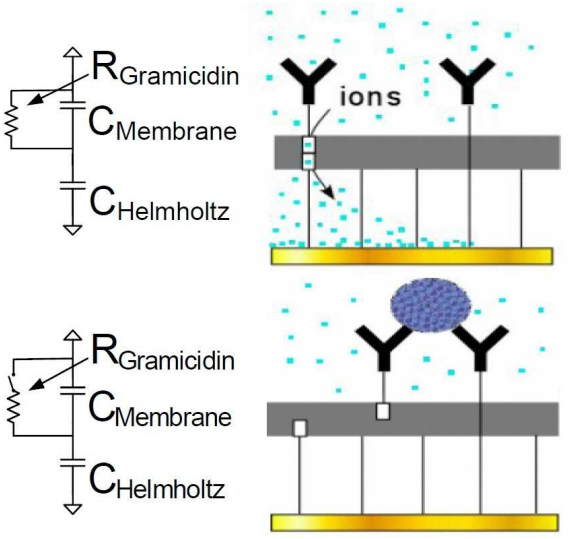

(a)

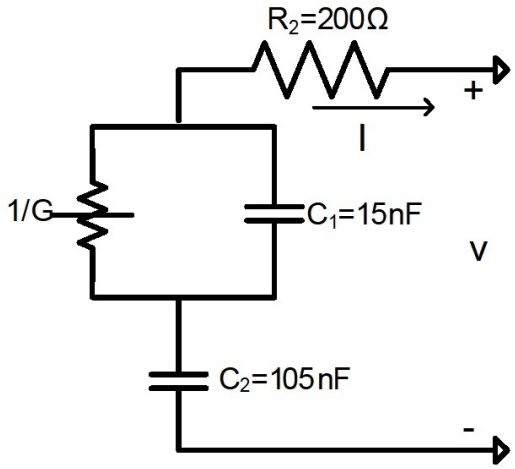

(b)

Figure 3.1: The ICS biosensor comprises of an ion channel switch. Fig.3.1(a) on top shows the switched-on state when the ion channels are conducting and on the bottom shows the switched-off state when the ion channels are not conducting. Fig.3.1(b) shows the equivalent electrical circuit with parameter values specified for electrode area of 0.03 cm^2.

Element	Value
Membrane Capacitance C_1	0.5μF/cm^2
Interfacial Capacitance C_2	3.5μF/cm^2
Biosensor Resistance $R_1 = 1/G$	60kΩ–600kΩ
Electrolyte Resistance R_2	200Ω

Table 3.1: Typical values for the components of the equivalent electrical circuit of the ICS biosensor, depicted in Fig.3.1(b). The area of the electrode is 0.03 cm^2.

Let V denote the external applied potential and I denote the output current as depicted in Fig.3.1(b). With $V(s)$ and $I(s)$ denoting the Laplace transforms, the admittance transfer function of the equivalent circuit is

$$H(s) = \frac{I(s)}{V(s)} = \frac{s^2 + s(1/R_1C_1)}{s^2R_2 + s(R_2/R_1C_1 + 1/C_1 + 1/C_2) + 1/R_1C_1C_2} \quad (3.1)$$

The resistance of the biosensor when no analyte is present is approximately 60kΩ. This can be reconciled with the $10^{11}\Omega$ per channel resistance of gramicidin A as follows. Since there are 10^8 gramicidin channels per cm^2, each electrode of area 0.03cm^2 contains approximately 3×10^6 channels with approximately half of them dimerized. So the effective resistance of all the dimerized ion channels (which act as parallel resistors) is approximately 60kΩ. The measured current is the average effect of the formation and dissociation of thousands of dimers and is approximately continuous-valued.

3.2 Chemical Dynamics of the Biosensor

This section formulates the dynamics of the chemical reactions in the biosensor with the goal of modeling how the biosensor conductance $G = 1/R_1$ in

Eq. (3.1) evolves. Recall that if analyte molecules are present, due to chemical reactions that inhibit the formation of gramicidin dimers, G decreases with time. In order to model the change in channel conductance in response to the introduction of analyte, it is necessary to model the chemical kinetics of the ICS biosensor. Experimental analysis of the biosensor shows that variations in G are faster and larger for large bulk analyte concentrations.

3.2.1 Chemical Reaction Network

The reactions involved in the ICS biosensor stem from binding of analyte molecules to the binding sites tethered to the gold electrode followed by cross-linking of the mobile ion channels to these bound analytes. The species involved in these reactions are separated into primary species and complexes. The primary species are analyte a with concentration A, binding sites b with concentration B, free moving monomeric ion channels c with concentration C, and tethered monomeric ion channels s with concentration S as shown in Fig. 1.1. The complexes denoted as d, w, x, y and z with concentrations, D, W, X, Y and Z are formed according to the following chemical reactions

$$\begin{aligned}
a &+ b \overset{f_1}{\underset{r_1}{\rightleftharpoons}} w && (a)\\
a &+ c \overset{f_2}{\underset{r_2}{\rightleftharpoons}} x && (b)\\
w &+ c \overset{f_3}{\underset{r_3}{\rightleftharpoons}} y && (c)\\
x &+ b \overset{f_4}{\underset{r_4}{\rightleftharpoons}} y && (d)\\
c &+ s \overset{f_5}{\underset{r_5}{\rightleftharpoons}} d && (e)\\
a &+ d \overset{f_6}{\underset{r_6}{\rightleftharpoons}} z && (f)\\
x &+ s \overset{f_7}{\underset{r_7}{\rightleftharpoons}} z && (g)
\end{aligned} \tag{3.2}$$

In Eqs. (3.2 a-g), f_i and r_i, for $i = \{1, 2, 3, 4, 5, 6, 7\}$, denote the *forward* and *backward* reaction rate constants respectively. For reactions occurring in 3 dimensional space (Eqs. (3.2 a,b,f)) the forward reaction rate constants, f_i, have units of $M^{-1}s^{-1}$ (M denotes molar concentration, i.e., moles per liter). For reactions occurring in 2 dimensional space, such as dimerization of the ion channel (Eq. (3.2 e)), f_i have units of $cm^2s^{-1}molecule^{-1}$. The backward reaction rate constants, r_i, have units of s^{-1} for all reactions.

The chemical reactions in Eqs. (3.2 a-g) give a complete symbolic description of the operation of the ICS biosensor that was qualitatively described in Section 2.3.

Solution containing analyte molecules, a, enters the biosensor flow chamber at $x_1 = 0$ where x_1 denotes the direction along the flow. Analyte concentration in the flow chamber is a function of x_1, x_2 and x_3 where x_3 denotes the direction perpendicular to the flow and x_2 denotes the direction along the width of the flow chamber. Analyte molecules are carried to the biosensor surface by advection and diffusion and interact with the immobilized species according to the chemical reactions denoted in Eqs. (3.2). The forward part of Eq. (3.2 a) reports on an analyte molecule a being captured by a binding site b and the resulting complex is denoted by w. Equation (3.2 c) shows that a free moving gramicidin monomer c in the outer leaflet of the bilayer lipid membrane (BLM), can bind to the complex w, thus producing another complex, denoted by y. An analyte molecule can also be captured by the binding site linked to the freely diffusing monomer, c. Equation (3.2 b) shows that this results in the production of the complex, x. The complex x can still diffuse on the outer leaflet of the BLM, move towards a tethered

binding site, b, and bind to it, resulting in the complex y (Eq. (3.2 d)). The biosensor conductance, $G(t)$, is proportional to the dimer concentration, $D(t)$. Therefore the event that determines the biosensor conductance is the formation of a conducting dimer, d, through the binding of the free moving ion channel monomer, c, and the tethered ion channel monomer, s, as shown in Eq. (3.2 e). An analyte molecule can also bind to an already formed dimer, which produces the complex z as shown in Eq. (3.2 f). Finally analyte bound to a free moving monomer can bind to a tethered monomer according to Eq. (3.2 g) to form z again.

We are now ready to formulate the chemical kinetics of the ICS biosensor. Using the law of mass action we can write rate equations describing the evolution of the concentration of the chemical species in the biosensor. For example, consider the primary species, b in Eqs. (3.2). According to Eqs. (3.2 a,d) b is consumed when it binds to a and x, and is produced when w and y decompose. So the change in the concentration of b, can be expressed as

$$\frac{dB}{dt} = -f_1 AB + r_1 W - f_4 XB + r_4 Y$$

The equations describing the evolution of the concentration of the other species can be derived similarly yielding Eq. (3.4). In order to put the equations in a more compact form we have used the following reaction rate expressions derived from Eqs. (3.2)

$$\begin{aligned} R_1 &= f_1 AB - r_1 W \quad R_2 = f_2 AC - r_2 X \\ R_3 &= f_3 WC - r_3 Y \quad R_4 = f_4 XB - r_4 Y \\ R_5 &= f_5 CS - r_5 D \quad R_6 = f_6 AD - r_6 Z \\ R_7 &= f_7 XS - r_7 Z. \end{aligned} \tag{3.3}$$

Define $u = \{B,\ C,\ D,\ S,\ W,\ X,\ Y,\ Z\}^T$, and $r(u(t)) = \{R_1, R_2, R_3, R_4, R_5, R_6, R_7\}^T$, where T denotes transpose and R_i are defined in Eq. (3.3). Then the system of nonlinear ordinary differential equations describing the evolution of the concentration of the chemical species is

$$\frac{du}{dt} = Mr(u(t)) \tag{3.4}$$

$$\text{where } M = \begin{pmatrix} -1 & 0 & 0 & -1 & 0 & 0 & 0 \\ 0 & -1 & -1 & 0 & -1 & 0 & 0 \\ 0 & 0 & 0 & 0 & 1 & -1 & 0 \\ 0 & 0 & 0 & 0 & -1 & 0 & -1 \\ 1 & 0 & -1 & 0 & 0 & 0 & 0 \\ 0 & 1 & 0 & -1 & 0 & 0 & -1 \\ 0 & 0 & 1 & 1 & 0 & 0 & 0 \\ 0 & 0 & 0 & 0 & 0 & 1 & 1 \end{pmatrix}$$

Initially ($t \leq 0$), $A = 0$ and the system is assumed to be in equilibrium. Therefore the initial conditions for the system of differential equations in

Initial Concentration of Species	**Value**
Mobile gramicidin A monomers C^*	10^8(molecules/cm^2)
Tethered gramicidin A monomers S^*	10^9(molecules/cm^2)
Tethered Binding Site B^*	10^8–10^{12}(molecules/cm^2)
Analyte A	(μM–fM)

Table 3.2: Prescribed concentrations of primary species in the ICS biosensor.

Eq. (3.4) are

$$\begin{aligned} B(0) &= B^* && (a) \\ C(0)+D(0) &= C^* && (b) \\ S(0)+D(0) &= S^* && (c) \\ f_5 S(0)C(0) &= r_5 * D(0) && (d) \\ W(0) &= 0 && (e) \\ X(0) &= 0 && (f) \\ Y(0) &= 0 && (g) \\ Z(0) &= 0 && (h) \end{aligned} \tag{3.5}$$

In Eqs. (3.5 a-c), B^*, C^*, S^* are the prescribed initial concentrations given in Table 3.2. In order to derive expressions for $D(0)$ and $C(0)$, from Eq. (3.5 d) we write

$$\frac{C(0)}{D(0)} = \frac{r_5}{f_5 S(0)}$$

Defining $\alpha = r_5/f_5 S(0) = r_5/f_5 S^*$ we find from Eq. (3.5 b) that

$$D(0) = \frac{C^*}{(1+\alpha)}, \quad C(0) = \frac{\alpha C^*}{(1+\alpha)} \tag{3.6}$$

Equation (3.4) with initial conditions given in Eq. (3.5) and Eq. (3.6) is a complete representation of the chemical kinetics of the biosensor.

Reaction Rate	Streptavidin-Biotin	hCG-IgG
$f_1 = f_2 = f_6$	10^7 ($M^{-1}s^{-1}$)	5×10^5 ($M^{-1}s^{-1}$)
$f_3 = f_4$	10^{-10} ($cm^2s^{-1}molecule^{-1}$)	5×10^{-11} ($cm^2s^{-1}molecule^{-1}$)
$f_5 = f_7$	10^{-11} ($cm^2s^{-1}molecule^{-1}$)	10^{-11} ($cm^2s^{-1}molecule^{-1}$)
$r_1 = r_2 = r_6$	10^{-6} (s^{-1})	10^{-4} (s^{-1})
$r_3 = r_4$	10^{-6} (s^{-1})	10^{-4} (s^{-1})
$r_5 = r_7$	5×10^{-3} (s^{-1})	10^{-2} (s^{-1})

Table 3.3: Typical values of the reaction rates f_i and r_i for antigen-antibody pair hCG-IgG and streptavidin-biotin pair. (hCG is Human chorionic gonadotropin, and IgG is Immunoglobin G. The concentration of the Glycoprotein hormone in a woman's blood or urine, increases by up to 10^5 during the early stages of pregnancy).

Table 3.3 gives typical forward and backward reaction rate constant values, (f_i, r_i), for two important examples. The first example is the interaction of proteins streptavidin and biotin. The second example in Table 3.3 deals with antigen-antibody interaction involving the detection of the pregnancy hormone (human chorionic gonadotropin (hCG)) by using the antibody Immunoglobin G (IgG) as the binding site of the biosensor. The simulations performed in this study involve the interaction of streptavidin and biotin, therefore the rate constants denoted for this interaction in Table 3.3 are used to simulate biosensor response in Chapter 4.

3.2.2 Black Box Model for Biosensor Response

The next step is to describe the input/output behavior of the biosensor. This can be viewed as a "black-box model" in comparison to the previous sections where physical/chemical laws were used to construct a "white-box" model. Let $n = 0, 1, \ldots$ denote discrete time (with typical sampling interval

of 1 second) and A denote the concentration of analyte. As described earlier, the presence of analyte results in a decrease of the biosensor conductance, G. Detailed experimental analysis of the biosensor response, show that G evolves in discrete time according to one of 3 different concentration modes; $\mathcal{M}$:

$$G_{n+1} = f^{\mathcal{M}}(G_n, A) + w_n, \tag{3.7}$$

$$\mathcal{M} = \begin{cases} 1 & A \text{ is low } : f^1(G_n, A) = G_n + \kappa_0 \\ 2 & A \text{ is medium} : f^2(G_n, A) = \kappa_1 G_n + \kappa_2 \\ 3 & A \text{ is high} : f^3(G_n, A) = \kappa_3 G_n + \kappa_4 \end{cases}$$

Here $\kappa_0, \kappa_1, \kappa_2, \kappa_3, \kappa_4$ are constants, with $|\kappa_1|, |\kappa_3| < 1$ to ensure stability of the system defined in Eq. (3.7). w_n is a noise process that models our uncertainty in the evolution of G. The function $f^{\mathcal{M}}$ models the fact that the biosensor conductance G_n decreases according to one of 3 distinct modes depending on the analyte concentration A. For low (or no) analyte present ($\mathcal{M} = 1$), the conductance decreases linearly. For medium and high concentrations ($\mathcal{M} = 2$, $\mathcal{M} = 3$), the decrease in conductance is exponential with different decay rates. High analyte concentration refers to ($A \geq 10^{-8}$M) and medium analyte concentration refers to ($A \geq 10^{-10}$M).

Fig. 3.2 shows examples of the experimental biosensor response to Streptavidin with different concentrations and provides a clear demonstration of the different kinetic regimes of the sensor function; see [1, 2] for details. The Streptavidin-biotin binding pair is one of the strongest and best character-

ized interactions available and is used as a model system in this project.

3.3 Analyte Flow and Biosensor Dynamics

Having formulated models for the electrical response and chemical kinetics, we are now ready to analyze these models to predict the ICS biosensor's response. The chemical kinetics of the biosensor are analyzed under two different operating conditions, the reaction-rate-limited and the mass-transport influenced operating conditions. The biosensor operation in the reaction-rate-limited region is described by the system of nonlinear ordinary differential equations denoted in Eq. (3.4) subject to initial conditions defined in Eqs. (3.5, 3.6). The biosensor response in the mass-transport influenced region is described by a partial differential equation coupled with a set of nonlinear ordinary differential equations through the boundary condition at $x_3 = 0$. The two models are described in detail in Section 3.3.1 and Section 3.3.2.

3.3.1 Reaction-Rate-Limited Kinetics

In the reaction-rate-limited regime, high bulk analyte concentrations, low binding site densities and large flow rates compensate for the depletion of analyte molecules due to reactions at the biomimetic surface populated by the binding sites. In this regime, it is reasonable to assume that the analyte concentration is approximately constant over space and time, i.e., $A(x_1, x_2, x_3, t) = A^*$, where A^* denotes the bulk analyte concentration. Therefore the chemical kinetics, under reaction-rate-limited operating con-

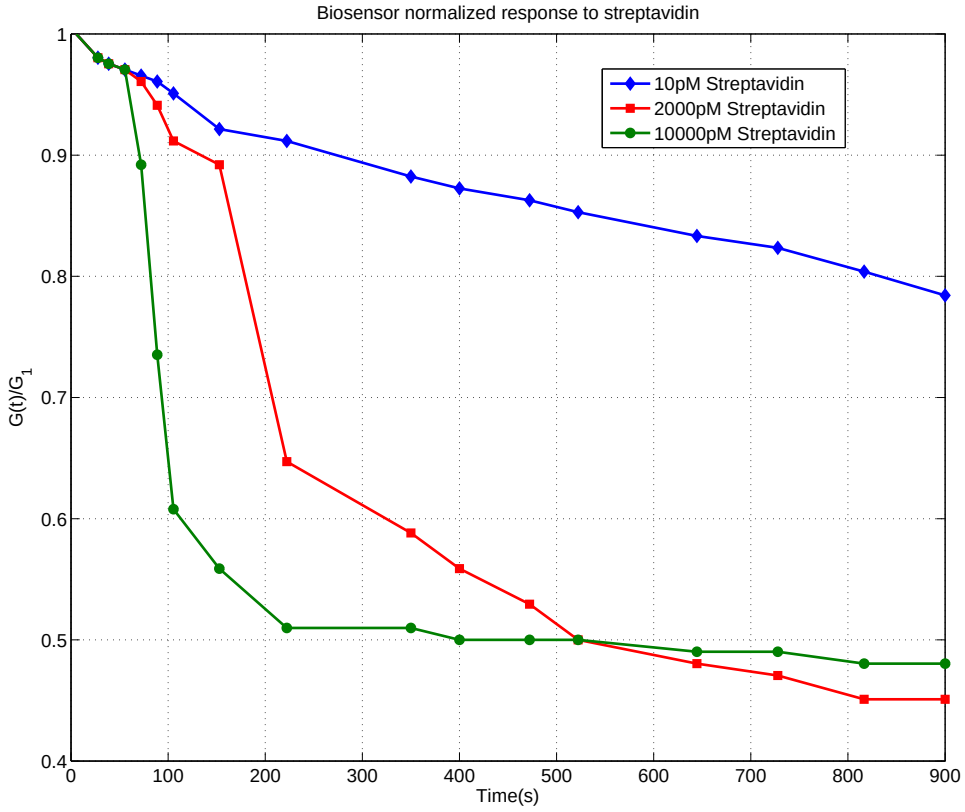

Figure 3.2: Experimental biosensor response (normalized decrease in channel conductance G) to Streptavidin . The figure demonstrates two experimentally observed modes of decay of the system conductance G depending on the analyte concentration, namely linear and exponential; see [1, 2] for details

ditions, are explained by Eq. (3.4) subject to initial conditions given in Eqs. (3.5, 3.6) with $A(x_1, x_2, x_3, t)$ replaced by A^*.

Under reaction-rate-limited operating conditions, the biosensor response is insensitive to flow rate. Fig. 3.3 shows quantitative predictions of the change in the biosensor resistance per unit time for various binding site densities and sample flow rates, for medium analyte concentrations (100pM) and low analyte concentrations (10fM). These are results predicted from the derived dynamical models for the operation of the ICS biosensor.

In Fig. 3.3 (a) biosensor response rate for medium analyte concentration (100pM) is shown to be independent of flow rate. Increasing the binding site density makes the mass transport effects more important. At higher binding site densities the biosensor response is slightly diminished for lower flow rates. However, increasing the flow rate improves the biosensor response only slightly.

3.3.2 Mass Transport Influenced Kinetics

When the ratio of analyte concentration to binding site density is small (e.g. $A/B = 1\text{pM}/10^{11} = 10^{-23}$), mass transport effects become the dominant criterion in achieving an acceptable response rate of the biosensor to analyte. Because the rate of transport of analyte molecules to the biosensor surface is comparable or slower than the chemical reaction rates, the analyte molecules lost due to chemical reactions are not replaced instantaneously. Therefore it is no longer valid to assume constant analyte concentration and instead the local concentration of analyte, $A(x_1, x_2, x_3, t)$, varies over space and time. In this section we model the change in analyte concentration over time and

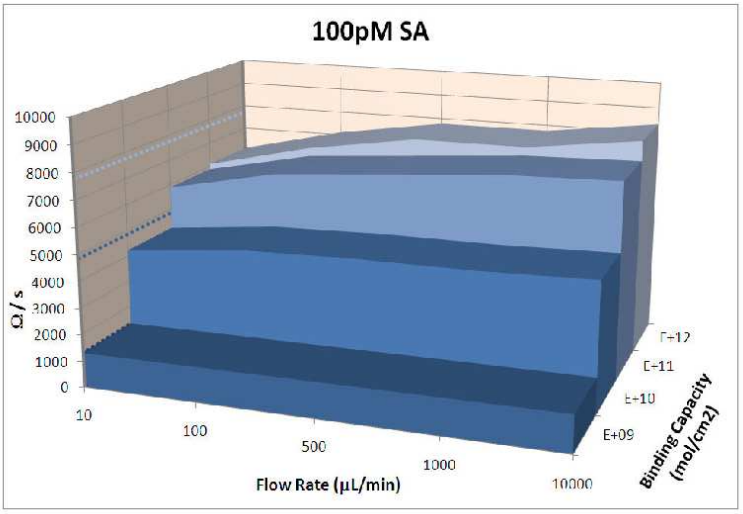

(a)

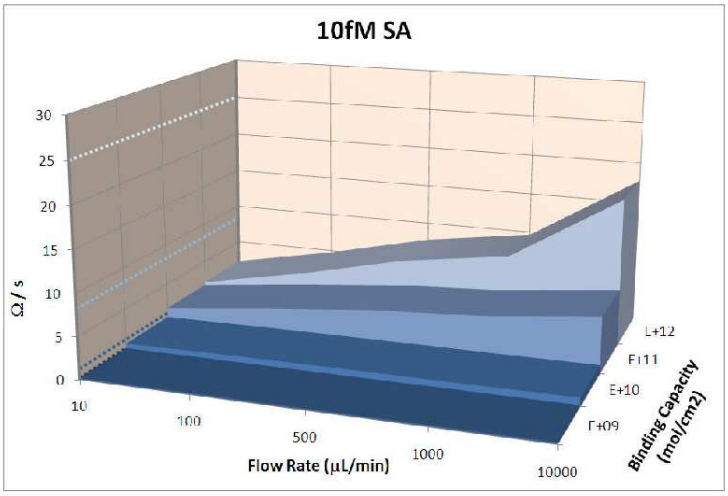

(b)

Figure 3.3: Biosensor response to 100pM and 10fM concentrations of Streptavidin for various binding site densities and flow rates. (a) At 100pM and low binding site densities, increasing the flow rate (left to right) has little effect on biosensor response. (b) At 10fM and low binding site densities there is no measurable biosensor response. At high binding site densities increasing the flow rate increases the biosensor response significantly.

space by a boundary value partial differential equation. We will start with a motivating example of why it is important to model the effects of mass transport on the biosensor response.

Whereas, Fig. 3.3 (a) shows biosensor response in the reaction-rate-limited region where it is insensitive to flow rate as described in the last section, Fig. 3.3 (b) shows biosensor response under mass-transport influenced operating conditions. In Fig. 3.3 (b), for low binding site densities there is no measurable biosensor response. As the binding site density is increased a high flow rate is required to achieve a measurable response. This corresponds to mass-transport influenced kinetics [53]. It is apparent from Fig. 3.3 (b) that a high binding site density is essential for high sensitivity in cases of low analyte concentration. With high binding site density, target molecules collide more frequently with receptors and are thus captured more quickly. The greater the ratio of binding site density to analyte concentration, the faster the response of the biosensor.

Analyte is transported to the reacting surface of the ICS biosensor, by diffusion and flow, where it reacts with the immobilized receptors. The flow chamber used for the biosensor has a rectangular cross section as shown in Fig. 3.4. We let t be the time, and we introduce cartesian coordinates with origin at the inlet, the x_1 axis along the direction of flow and the x_3 axis perpendicular to the biospecific surface.

Along the flow chamber the velocity profile is fully developed, i.e. equals zero at the top ($x_3 = h$) and bottom ($x_3 = 0$) and reaches a maximum $\overline{\nu}$ in the center [54]. The velocity ν at height x_3 above the sensor surface is given

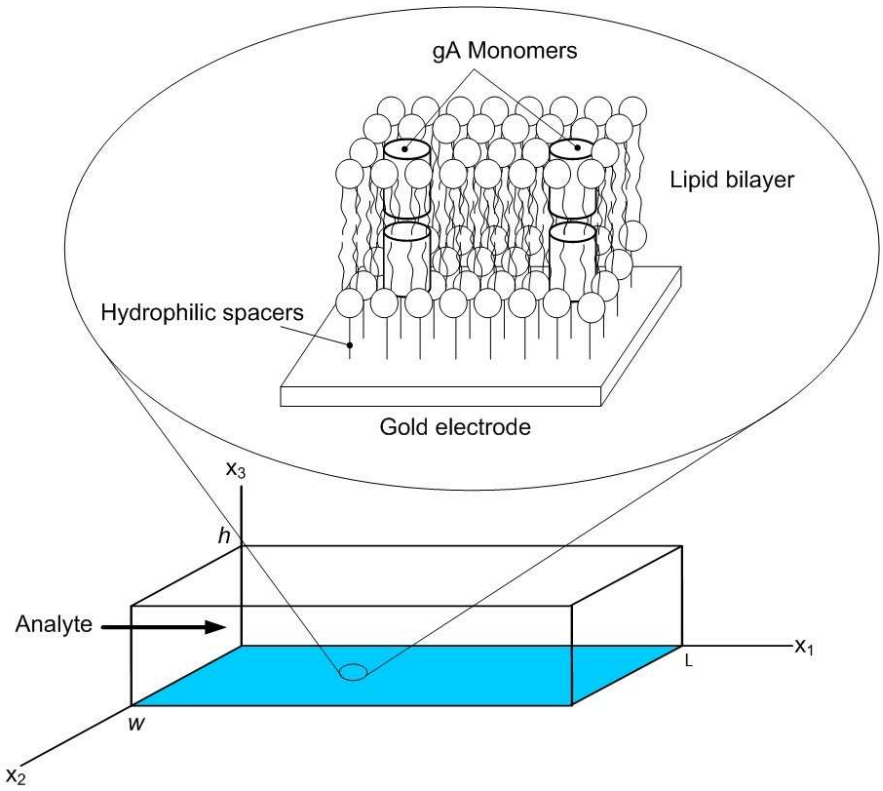

Figure 3.4: A schematic of the flow chamber, where the bio-specific surface is at $x_3 = 0$. The current generation of the ICS biosensor has $h = 0.1$mm, $W \approx 2$mm and $L \approx 2$mm. The figure is not to scale.

by

$$\nu(x_3) = 4\overline{\nu}(x_3/h)(1 - (x_3/h)) \tag{3.8}$$

The width of the flow chamber is 20 times its height, therefore we can ignore variations in the concentration along the x_2 axis [54]. The governing two dimensional parabolic partial differential equation (PDE) is

$$\frac{\partial A}{\partial t} = \gamma \left(\frac{\partial^2 A}{\partial x_1^2} + \frac{\partial^2 A}{\partial x_3^2} \right) - \nu(x_3) \frac{\partial A}{\partial x_1} \tag{3.9}$$

where $\nu(x_3)$ is given by Eq. (3.8) and $\gamma = 10^{-6}\text{cm}^2/\text{s}$ is the analyte diffusion coefficient [34], [55]. The boundary conditions for Eq. (3.9) are as follows.

- The concentration of the analyte at the inlet, $x_1 = 0$, is equal to the injection concentration A^*

$$A(x_1 = 0, x_3, t > 0) = A^* \tag{3.10}$$

- At the end of the flow chamber, $x_1 = L$, we assume that the exit of analyte is due entirely to flow and thus the flux of analyte at $x_1 = L$ can be taken to be zero

$$\frac{\partial A(x_1 = L, x_3, t > 0)}{\partial x_1} = 0 \tag{3.11}$$

- The chamber boundary at $x_3 = h$ is reflective and the mass flux must equal zero

$$\frac{\partial A(x_1, x_3 = h, t > 0)}{\partial x_3} = 0 \tag{3.12}$$

- At $x_3 = 0$, the mass flux must equal the rate by which analyte molecules are used. Analyte molecules are used in reactions denoted in Eqs. (3.2 a,b,f). Thus the boundary condition at $x_3 = 0$ is

$$\gamma \frac{\partial A(x_1, x_3 = 0, t > 0)}{\partial x_3} = -A\left(f_1 B + f_2 C + f_6 D\right) + r_1 W + r_2 X + r_6 Z \tag{3.13}$$

In the mass-transport influenced region of operation, the analyte concentration, $A(x_1, x_3, t)$, is obtained by solving Eq. (3.9) subject to the boundary conditions defined in Eqs. (3.10-3.13). However, since Eq. (3.13) involves the concentration of the other surface chemical species, the complete PDE model is coupled to the set of nonlinear ODEs defined in Eq. (3.4) in Section 3.2.1.

In the next section we will show through comparison of experimentally obtained biosensor response and simulated biosensor response that the derived mathematical models are valid under appropriate operating conditions.

Chapter 4

Model Evaluation

How good are the models described in the previous chapter in predicting the ICS biosensor's response? We defined the chemical reaction dynamics of the ICS biosensor in Section 3.2.1 with Eq. (3.4) subject to initial conditions given in Eqs. (3.5, 3.6). The analyte concentration A in these equations is both a function of space and time. However, depending on the operating conditions of the ICS biosensor, simplifications to this model are possible. The operating conditions of the ICS biosensor, i.e. analyte concentration, flow rate, and binding site densities, distinguish two operating regions, the reaction-rate-limited and the mass-transport influenced regions. The reaction-rate-limited region is achieved when high analyte concentrations, low binding site density and high flow rates are used. The mass-transport influenced operating conditions are approached when analyte concentration is low relative to the binding site density and flow rate is also low. The representative mathematical models of the system dynamics under these two operating conditions are derived in Section 3.3.1 and 3.3.2. In the next two sections, the derived mathematical models are numerically solved to simulate the biosensor response. The simulated response is then compared to experimentally obtained bisoensor response in order to verify the validity of

the derived models under appropriate operating conditions.

4.1 Reaction-Rate-Limited Kinetics

In this region of operation the analytical biosensor response is obtained by numerically solving the system of nonlinear differential equations denoted in Eq. (3.4) subject to initial conditions denoted in Eqs. (3.5, 3.6). Since the rate of transport of analyte to the sensor surface is fast compared to reaction rates as described in Section 3.3.1 we can assume $A(x_1, x_2, x_3, t) = A^*$. Solving this system of nonlinear differential equations numerically we can find $D(t)$. Since $D(t) \propto G(t)$, where $G(t)$ is the biosensor conductance, we can simulate the biosensor response under reaction-rate-limited operating conditions using this model. To show that the derived model in the reaction-rate-limited region of operation represents the dynamics of the ICS biosensor accurately, we conducted experiments on the biosensor for detecting streptavidin at 0.1nM concentrations. Biotin was used as the binding site with density $B = 2 \times 10^{11}$molecules/cm^2 and flow rate used was 100μL/min. In calculating the analytical response of the biosensor, reaction rate constants for the streptavidin-biotin interaction denoted in Table 3.3 were used. The results are demonstrated in Fig. 4.1. As shown in this figure the experimentally obtained biosensor response compares well with the analytical response, thus confirming the accuracy of the derived model under reaction-rate-limited operating conditions.

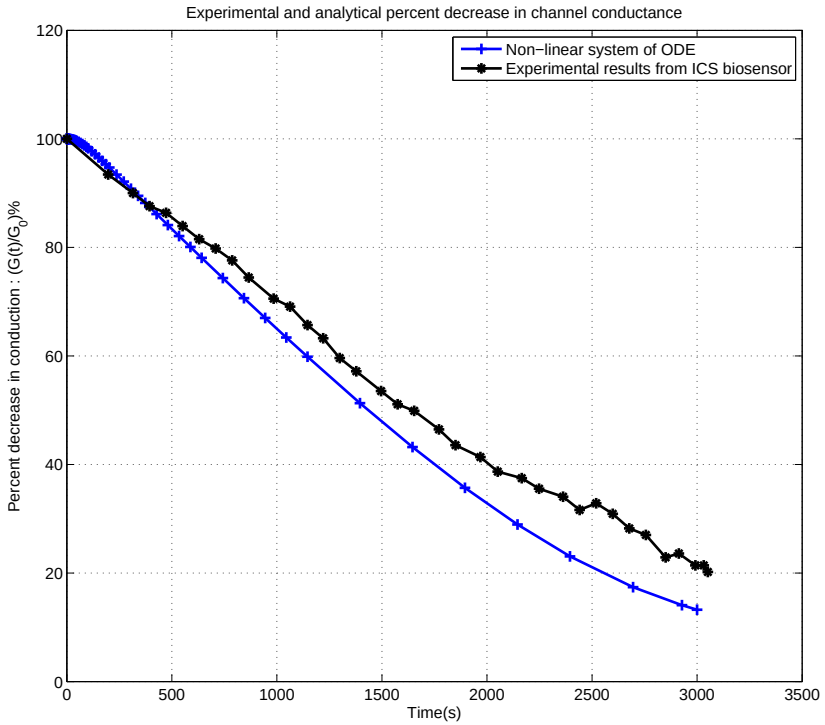

Figure 4.1: Response of ICS biosensor for $A^* = 0.1\text{nM}$, $B = 2 \times 10^{11}\text{molecules/cm}^2$ and flow rate= $100\mu\text{L/min}$. Both experimental (-*-) and analytical (-+-) results are shown. The blue (-+-) line demonstrates the biosensor response found from solving Eqs. (3.4, 3.5, and 3.6).

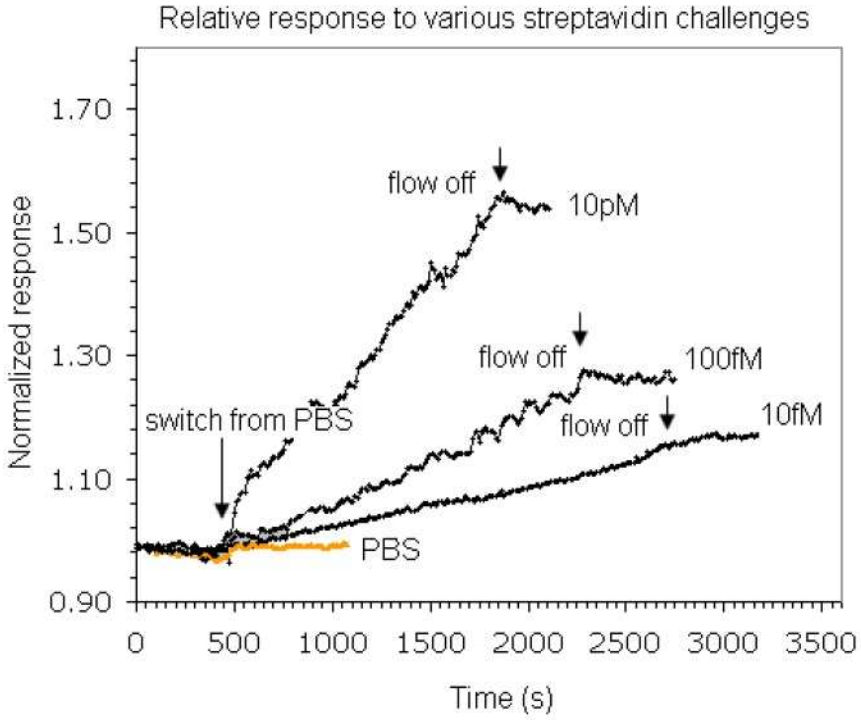

Figure 4.2: Experimental normalized increase in ICS biosensor resistance for the concentrations shown and 150μL/min flow rate. When the flow stops (indicated by arrows in the figure) the response stops at all concentrations. This is due to analyte depletion at the sensor surface.

4.2 Mass Transport Influenced Kinetics

We conducted experiments on the ICS biosensor in which a bolus of Streptavidin at 10fM, 100fM or 10pM was added to the feed line, at a constant flow rate of 150μL/min. Fig. 4.2 shows the biosensor normalized resistance as a function of time for the mentioned analyte concentrations.

Fig. 4.2 illustrates the sensitivity of the biosensor response in the mass transport region of operation to analyte concentration and flow rate. It is seen in this figure that as the analyte concentration is increased, the biosen-

sor exhibits faster response. It also shows that when the flow is stopped (as indicated by the arrows in the figure), the resistance increase stops. Restarting the flow causes the resistance rise to recommence, indicating the importance of flow rate on the biosensor response.

The experimentally measured response rate of the biosensor was compared with that predicted by our model denoted in Section 3.3.2. We computed the predicted response as follows: The mass-transport effects were computed by solving Eq. (3.9) subject to boundary conditions given in Eqs. (3.10-3.13) via finite element method on the rectangular flow cell shown in Fig. 3.4. The chemical kinetics were computed by solving Eq. (3.4) numerically. This yields the dimer concentration $D(t)$ and thus the biosensor conductance $G(t)$. Fig. 4.3 shows the experimentally measured response rate (black stars) to 10fM streptavidin at various flow rates from 0μL/min to 300μL/min. Also shown (pink diamond) is the theoretical response rate predicted by our model. As can be seen by eyeballing the plots, the predicted performance of the biosensor closely matches the experimental performance.

Fig. 4.3 also shows the predicted response rates from the reaction-rate-limited model for various flow rates (blue square). As expected the response rate predicted from reaction-rate-limited model is insensitive to flow rates. The resistance change, predicted by the reaction-rate-limited model, is almost three times the magnitude of the experimental change experienced at 100μL/min. This difference shows the necessity of the full partial differential equation in determining biosensor response in the mass-transport influenced region.

Finally, Fig. 4.4 shows the predicted and experimental response rate

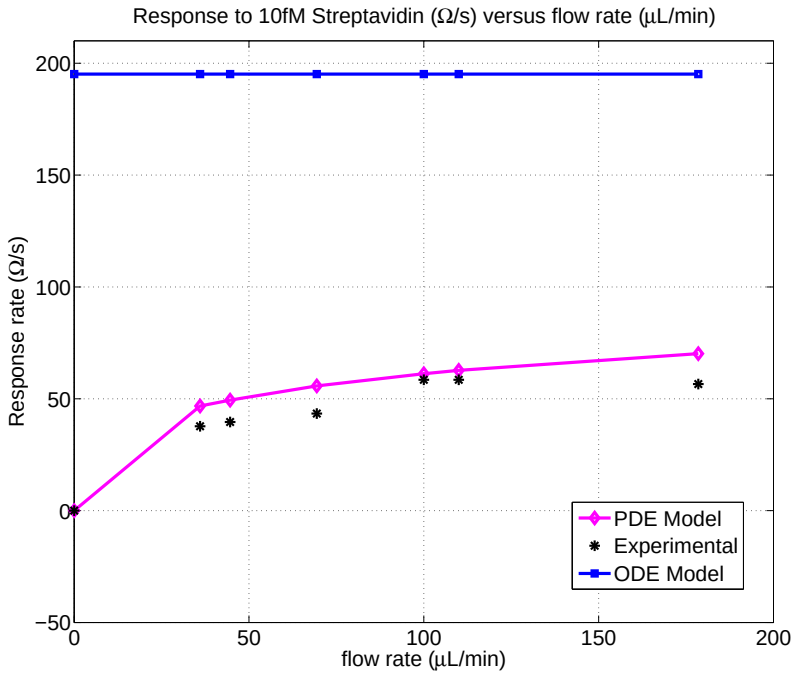

Figure 4.3: Response rate (Ω/s) of ICS biosensor to 10fM streptavidin with varying flow rates. Black stars show the experimental response rate of the biosensor as the flow rate is increased. The pink diamond line is the response rate predicted by the PDE model. The straight blue square line is the high flow response limit predicted by the reaction-rate-limited model.

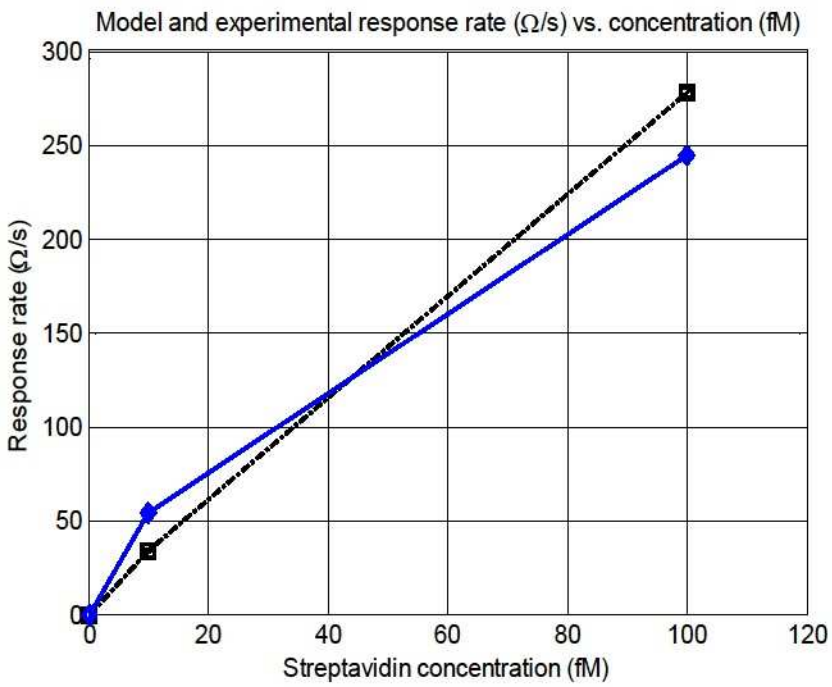

Figure 4.4: Predicted (blue diamonds) and experimental (black squares) titration curves for the ICS sensor response to Streptavidin in the range 1fM -100fM at 150μL/min. The black squares are experimental data and the blue diamonds are from the model.

in the range of 0fM to 100fM streptavidin. It confirms that the biosensor response rate increases with analyte concentration.

Chapter 5

Conclusion and Future Work

This chapter provides a summary of the work accomplished in this project, as well as provides a summary of possible future extensions to this project.

5.1 Summary of Work Accomplished

This thesis considers the problem of derivation of accurate mathematical models that describe the dynamics of a fluidic-based solid phase immunoassay biosensor, calleds the Ion Channel Switch (ICS) biosensor, under various operating conditions.

In the ICS biosensor variations in the channel conductance report on the presence and concentration of the analyte present in the sample solution. Since the presence of analyte disrupts the ability of gA ion channels to align and form conducting dimers, the channel conductance is proportional to the concentration of the dimers in the biosensor. Therefore in order to model the biosensor response, the chemical reaction network of the ICS biosensor needs to be studied. In this thesis the electrical as well as chemcial dynamics of the ICS biosensor are mathematically modelled and compared to experimental data obtained from ICS biosensor.

The electrical dynamics of the ICS biosensor are modelled by an equiva-

lent electrical circuit, whose parameter values are related to sensor operation and structure.

In the ICS biosensor, analyte is transported by advection and diffusion to the biosensor surface where it interacts with the immobilized species on the biosensor surface according to the reactions denoted in the chemical reaction network of the system. The transport of analyte to the biosensor surface is modelled by a two dimensional, advection diffusion partial differential equation subject to a mixture of Neumann and Dirichlet boundary conditions. The boundary condition at the bottom of the rectangular cross section flow chamber of the biosensor, in particular, highlights the binding of analyte to the immobilized species. The evolution of the concentration of the chemical species on the biosensor surface are found from the biosensor reaction network by using the law of mass action. We arrive at a system of nonlinear ordinary differential equations that describes the rate of change of the concentration of the chemical species in the biosensor including the dimer concentration which reports on the channel conductance. The partial differential equation coupled with the system of nonlinear ordinary differential equations on the biosensor surface, provides an accurate mathematical model that predicts the biosensor behaviour under all possible operating conditions. However, by considering the operating conditions which include, analyte concentration, binding site density, dimensions of the flow chamber as well as the flow rate, two regions of operation are distinguished; the reaction-rate-limited and the mass-transport limtied regions.

In the reaction-rate-limited region, large flow rates, high alyte concentrations or low binding site densities compensate for the depletion of analyte

at the surface due to chemical reactions. In this region it is reasonable to assume constant analyte concentration which decouples the partial differential equation from the set of nonlinear ordinary differential equations. Therefore the set of nonlinear ordinary differential equations with $A(x_1, x_3, x_2, t)$ replaced by the bulk analyte concentration A^* represents the dynamics of the biosensor in this region of operation. Numerical studies verify the accuracy of this model under appropriate operating conditions.

On the other hand in the mass-transport influenced region the rate of transport of analyte to the biosensor surface is slower than or comparable to the surface reaction rates. Therefore it is no longer valid to assume constant analyte concentration. In this region the full system, consisting of the partial differential equation coupled with the set of nonlinear ordinary differential equations, needs to be solved numerically to accurately simulate the biosensor response. Comparison of simulated biosensor response with the experimental data obtained under appropriate operating conditions, confirms the accuracy of the model.

Therefore the dynamics of the biosensor are represented accurately under both operating regimes using the derived mathematical models.

5.2 Future Work

1. **Analytical equations for ICS biosensor conductance :** Since most biochemical reaction networks possess multiple time scales due to the different rate constants involved in the reactions, it might be possible to simplify the system of nonlinear ordinary differential equations

in the reaction-rate-limited region of operation to arrive at analytical equations describing evolution of the dimer concentration, $D(t)$. This would in turn provide analytical equations for channel conductance $G(t)$. Using typical parameter values for streptavidin-biotin interaction we discovered that the linearized system of nonlinear ordinary differential equations possesses eigenvalues with vastly different values. This indicates the existence of different time scales in the system. Using methods such as Computational Singular Perturbation (CSP) or the Intrinsic Low Dimensional Manifolds (ILDM) , it is possible to determine the fast and slow species in the chemical reaction network [56]. This allows us to reduce the number of differential equations thus reducing the complexity of the studied biochemical system. Grouping the fast and slow chemical species allows us to cast the system of differential equations into the singularly perturbed form. Then we can apply singular perturbation analysis to the simplified system and try to arrive at analytical equations for $G(t)$. Analytical equations for $G(t)$ can be used as the state equation in optimization and classification problems as well.

2. **Obtaining kinetic parameters :** Solid phase immunoassay biosensors, such as BIACORE, have traditionally been used to study the interaction between biomolecules. In order to obtain intrinsic reaction rate constants from binding data, a mathematical model needs to be fitted to the data. The partial differential equation denoted in Eq. (3.9), and its boundary conditions, Eqs. (3.10-3.13) present an

impractical model for this purpose. A simpler mathematical model is required to accurately simulate binding data as well as lend itself to estimation algorithms. Models such as the two compartment model have previously been used to simulate the binding data of solid phase immunoassay biosensors in the mass-transport influenced region [11], [10]. However, the biosensor operation in all the studied cases is much simpler than the ICS biosensor. For example in BIACORE, there is only one reaction occurring at the surface, the binding of analyte to the receptor molecules, whereas in the ICS biosensor there are seven simultaneous chemical reactions occurring on the biosensor electrode. Adapting the two compartment model to be applied to the ICS biosensor is worth pursuing since ICS biosensor presents an alternative technology to BIACORE sensor in analyzing biomolecular interactions.

Bibliography

[1] B. Cornell, "Membrane-based biosensors," in *Optical biosensors: Present and future*, F.S. Ligler and C.A.R. Taitt, Eds., p. 457. Elsevier, 2002.

[2] G. Woodhouse, L. King, L. Wieczorek, P. Osman, and B.Cornell, "The ion channel swtich biosensor," *Journal of Molecular Recognition*, vol. 12, no. 5, pp. 328 –334, 1999.

[3] R. Baronas, F. Ivanauskas, and J. Kulys, "Modelling dynamics of amperometric biosensors in batch and flow injection analysis," *Journal of Mathematical Chemistry*, vol. 32, no. 2, pp. 225–237, 2002.

[4] D. Grieshaber, R. Mackenzie, J. Voros, and E. Reimhult, "Electrochemical biosensors - sensor principles and architectures," *Sensors*, vol. 8, pp. 1400–1458, 2008.

[5] B. M. Paddle, "Biosensors for chemical and biological agents of defence interest," *Biosensors and Bioelectronics*, vol. 1, no. 11, pp. 1079–1113, 1996.

[6] A.M. Aliakbar, "Handheld impedance based biosensor system for glucose monitoring," M.S. thesis, McGill University, 2009.

[7] *Biosensors : Theory and Applications*, Technomic Publishing Company Inc., 1993.

[8] A. Ramakrishnan and A. Sadana, "Analytereceptor binding kinetics for biosensor applications: A single-fractal and a dual-fractal analysis of the influence of the fractal dimension on the binding rate coefficient," *Journal of Colloid and Interface Science*, vol. 208, pp. 455–467, 1998.

[9] T. Mason, A.R. Pineda, C. Wofsy, and B. Goldstein, "Effective rate models for the analysis of transport-dependent biosensor data," *Mathematical Bioscience*, vol. 159, pp. 123–144, 1999.

[10] D.G. Myszka, H. Xiaoyi, D. Micah, T.A. Morton, and B. Goldstein, "Extending the ragne of rate constants available from biacore: Interpreting mass transport-influenced binding data," *Biophysical Journal*, vol. 75, pp. 583–594, 1998.

[11] D.G. Myszka, T.A. Morton, M.L. Doyle, and I.M. Chaiken, "Kinetic analysis of a protein antigen-antibody interaction limited by mass transport on an optical biosensor," *Biophysical Chemistry*, vol. 64, pp. 127–137, 1997.

[12] B. Cornell, V.L. Braach-Maksvytis, L.G. King, P.D. Osman, B. Raguse, L. Wieczorek, and R.J. Pace, "A biosensor that uses ion-channel switches," *Nature*, vol. 387, pp. 580–583, 1997.

[13] E. Neher, "Molecular biology meets microelectronics," *Nature Biotechnology*, vol. 19, Feb 2001.

[14] D. Georganopoulou, "Reagentless electrochemical biosensors for clinical diagnostics," in *41st Annual Oak Ridge Conference*, Baltimore, April 2009, Frontiers in Clinical Diagnostics.

[15] M.C. Peterman, J.M. Ziebarth, O. Braha, H. Bayley, H.A. Fishman, and D.M. Bloom, "Ion channels and lipid bilayer membranes under high potentials using microfabricated apertures," *Biomedical Microdevices*, vol. 4, pp. 236–236, 2002.

[16] S. Howorka, J. Nam, H. Bayley, and D. Kahne, "Stochastic detection of monovalent and bivalent protein-ligand interactions," *Angew. Chem. Int. Ed.*, vol. 43, pp. 842–846, 2004.

[17] F.S. Ligler, T.L. Fare, E.E. Seib, J.W. Smuda, A. Singh, P. Ahl, M.E. Ayers, A.W. Dalziel, and P. Yager, "Fabrication of key components of a receptor-based biosensor," *Med. Instrumentation*, vol. 22, pp. 247–256, 1988.

[18] R. Naumann, E.K. Schmidt, A. Jonczyk, K. Fendler, B. Kadenbach, T. Liebermann, A. Offenhausser, and W. Knoll, "The peptide-tethered lipid membrane as a biomimetic system to incorporate cytochrome c oxidase in a functionally active form," *Biosensors and Bioelectronics*, vol. 14, no. 7, pp. 651–662, 1999.

[19] J. Li-Fries, *Ion Channels in Mixed Tethered Bilayer Lipid Membranes*, Ph.D. thesis, Max Planck Institut fr Polymerforschung, 2007.

[20] S. Heysel, H. Vogel, M. Sanger, and H. Sigrist, "Covalent attachment of functionalized lipid bilayers to planar waveguides for measuring protein

binding to biomimetic membranes," *Protein Science*, vol. 4, no. 12, pp. 2532–2544, 1995.

[21] X.D. Lu, A.L. Ottova, and H.T. Tien, "Biophysical aspects of agar-gel supported bilayer lipid nembranes: a new method for forming and studying planar bilayer lipid membranes," *Bioelectrochemistry and Bioenergetics*, vol. 39, no. 2, pp. 285–289, 1996.

[22] C. A. Naumann, W. Knoll, and C.W. Frank, "Hindered diffusion in polymer-tethered membranes: A monolayer study at the air-water interface," *Biomacromolecules*, vol. 2, no. 4, pp. 1097–1103, 2001.

[23] C. Steinem, A. Janshoff, W.P. Ulrich, M. Sieber, and H.J. Galla, "Impedance analysis of supported lipid bilayer membranes: a scrutiny of different preparation techniques," *Biochimica et Biophysica Acta.*, vol. 1279, pp. 169–180, 1996.

[24] E. Sackmann, "Supported membranes: Scientific and practical applications," *Science*, vol. 271, pp. 43–48, 1996.

[25] A.L. Plant, "Supported hybrid bilayer membranes as rugged cell membrane mimics," *Langmuir*, vol. 15, pp. 5128–5135, 1999.

[26] K. Motesharei and M.R. Ghadiri, "Diffusion-limited size-selective ion sensing based on SAM-supported peptide nanotubes," *Journal of the American Chemical Society*, vol. 119, pp. 11306–11312, 1997.

[27] F. Separovic and B. Cornell, "Gated ion channel-based biosensor de-

vice," in *Biological Membrane Ion Channels*, S.H. Chung, O. Andersen, and V. Krishnamurthy, Eds., pp. 595–621. Springer-Verlag, 2007.

[28] J. Bufler, S. Kahlert, S. Tzartos, A. Maelicke, and C. Franke, "Activation and blockade of mouse muscle nicotinic channels by antibodies directed against the binding site of the acetylcholine receptor," *Journal of Physiology-London*, vol. 492, April 1996.

[29] A.N. Lopatin, E.N. Makhina, and C.G. Nichols, "The mechanism of inward rectification of potassium channels: long-pore plugging by cytoplasmic polyamines," *Journal of General Physiology*, vol. 106, pp. 923–955, Nov 1995.

[30] T. Stora, J.H. Lakey, and H. Vogel, "Ion-channel gating in transmembrane receptor proteins: Functional activity in tethered lipid membranes," *Angewandte Chemie International Edition*, vol. 38, pp. 389–392, 1999.

[31] B. Hille, *Ionic Channels of Excitable Membranes*, Sinauer Associates, Inc., Sunderland, MA., 3 edition, 2001.

[32] K. Cole, *A Quantitiative Description of Membrane Current and its application to conductance and excitation in nerve*, University of California Press, Berkeley, 1968.

[33] D. Lauffenburger and J.K. Linderman, *Receptors–Models for Binding, Trafficking and Signaling*, Oxford, 1993.

[34] David A. Edwards, "Estimating rate constants in a convection-diffusion

system with a boundary reaction," *IMA Journal of Applied Mathematics*, vol. 63, pp. 89–112, 1999.

[35] B. Goldstein, D. Coombs, X. He, A.R. Pineda, and C. Wofsy, "The influence of transport on the kinetics of binding to surface receptors: application to cell and BIAcore," *Journal of Molecular Recognition*, vol. 12, pp. 293–299, 1999.

[36] R.W. Glaser, "Antigen-antibody binding and mass transport by convection and diffusion to a surface: A two-dimensional computer model of binding and dissociation kinetics," *Analytical Biochemistry*, vol. 213, pp. 152–161, 1993.

[37] S. Qian and H.H. Bau, "A mathematical model of lateral flow bioreactions applied to sandwich assays," *Analytical Biochemistry*, vol. 322, pp. 89–98, 2003.

[38] S. Moldoveunu and J.L. Anderson, "Amperometric response of a rectangular channel electrode," *Journal of Electro-analytical Chemistry*, vol. 175, pp. 67–77, 1984.

[39] K. Lebedev and S.Mafe, "Convection, diffusion and reaction in a surface-based biosensor: Modeling of cooperativity and binding site competition on the surface and in the hydrogel," *Journal of Colloid and Interface Science*, vol. 296, pp. 527–537, 2006.

[40] P.Y. Lagree and A.I. Fernolendt, "Direct comparison of simplified models of surface reacting flows in flow chambers," *The European Physical Journal - Applied Physics*, vol. 26, pp. 133–143, 2004.

[41] S.R. Reiken, B.J. Vanwie, H. Sutisna, D.F. Moffett, A.R. Koch, M. Silber, and W.C. Davis, "Bispecific antibody modulation of nicotine acetylcholine receptors for biosensing," *Biosensors and Bioelectronics*, vol. 11, pp. 91–102, 1996.

[42] W.R. Veatch, E.T. Fossel, and E.R. Blout, "The conformation of gramicidin a," *Biochemistry*, vol. 13, pp. 5249–5256, 1974.

[43] S.H. Chung, O. Anderson, and V. Krishnamurthy, Eds., *Biological Membrane Ion Channels: Dynamics, Structure and Applications*, Springer-Verlag, 2007.

[44] V. Krishnamurthy and S.H. Chung., "Large-scale dynamical models and estimation for permeation in biological membrane ion channels," *Proceedings of the IEEE*, vol. 95, no. 5, pp. 853–880, May 2007.

[45] G. Woodhouse, L.G. King, and B.A. Cornell., "Kinetics of the competitive response of receptors immobilised to ion-channels which have been incorporated into a tethered bilayer," *Faraday Discussion*, vol. 111, pp. 247 –258, 1999.

[46] R.D. Hotchkiss and R.J. Dubois, "Fractionation of bactericidal agent from cultures of a soil bacillus," *Journal of Biological Chemistry*, vol. 132, pp. 791–792, 1940.

[47] B.A. Wallace, "Recent advances in the high resolution structures of bacterial channels: Gramicidin A," *Journal of Structural Biology*, vol. 121, no. 2, pp. 123–141, 1998.

[48] S.C. Kushwaha, M. Kates, G.D. Sprott, and I.C. Smith, "Novel complex polar lipids from the methanogenic archaebacterium methanospirillum hungatei," *Science*, vol. 211, pp. 1163–1164, 1981.

[49] M. De Rosa, M.A. Gamacorta, B. Nicolaus, B. Chappeand, and P. Albrecht, "Isoprenoid ethers; backbone of complex lipids of the archaebacterium sulfolobus solfataricus," *Biochimica et Biophysica Acta.*, vol. 753, pp. 249–256, 1983.

[50] A. Gliozzi, R. Rolandi, M. De Rosa, and A. Gamacorta, "Monolayer black membranes from bipolar lipids of archaebacteria and their temperature-induced structural changes," *Journal of Membrane Biology*, vol. 75, no. 1, pp. 45–56, 1983.

[51] R. Naumann, E.K. Schmidt, A. Jonczyk, K. Fendler, B. Kadenbach, T. Liebermann, D. Philip, and J.F. Stoddart, "Self-assembly in natural and unnatural systems," *Angewandte Chemie International Edition*, vol. 35, no. 11, pp. 1154–1196, 1996.

[52] G. Krishna, J. Schulte, B.A. Cornell, R. Pace, L. Wieczorek, and P.D. Osman, "Tethered bilayer membranes containing ionic reservoirs: The interfacial capacitance," *Langmuir*, vol. 17, pp. 4858–4866, 2001.

[53] R.A. Vijayendran, F.S. Ligler, and D.E. Leckband, "A computational reaction-diffusion model for analysis of transport-limited kinetics," *Journal of Analytical Chemistry*, vol. 71, pp. 5405–5412, 1999.

[54] J.P. Brody, P. Yager, R.E. Goldstein, and R.H. Austin, "Biotechnology

at low reynolds numbers," *Biophysical Journal*, vol. 71, pp. 3430–3441, 1996.

[55] B.K Lok, Y. Cheng, and C.R. Robertson, "Protein adsorption on crosslinked polydimethylsiloxane using total interanal reflection fluorescence," *Journal of Colloid and Interface Science*, vol. 91, no. 1, pp. 104–116, January 1983.

[56] I. Surovtsova1, N. Simus, T. Lorenz, A. Konig, S. Sahle, and U. Kummer, "Accessible methods for the dynamic time-scale decomposition of biochemical systems," *System biology*, vol. 25, no. 21, pp. 2816–2823, 2009.